

Geophysical characterization and modeling of a Neoproterozoic intrusive volcanoclastic lamprophyre in southernmost Brazil

Anderson Baesso^{1*} , Carlos Augusto Sommer¹ , Jairo Francisco Savian¹ ,
Johnathan Henrique Gambeta¹ , Robson dos Santos Aquino¹ 

Abstract

Neoproterozoic spessartitic lamprophyres are linked to the Lavras do Sul Shoshonitic Association in the Sul-Riograndense Shield, southernmost Brazil. Bodies of intrusive spessartitic lamprophyres occur in trachyandesites of this association in the Cerro Tupanci region. There, Neoproterozoic igneous and metamorphic complexes are covered by volcanic-sedimentary Ediacaran sequences of the Camaquã Basin that include trachyandesites, conglomerates, sandstones, and spessartitic lamprophyre dikes of which a spessartitic lapilli tuff N-NE oriented is the main occurrence. Gamma spectrometric and gravimetric data for the lapilli tuff allowed definition of its occurrence as a dike elongated N-S, bearing low values for gamma spectrometry and a strong negative gravimetric anomaly approximately 450 m long and 70 m wide. Two-dimensional modeling of this anomaly suggests that the dike is subvertical to vertical. Magnetometry did not provide significant data regarding the lamprophyre but did show a normal dipolar anomaly to the west, suggesting the presence of a non-outcropping cylindrical intrusion in the area.

KEYWORDS: gamma spectrometry; gravimetry; magnetometry; geophysical modeling;

INTRODUCTION

The occurrence of mineralizations associated to lamprophyric rocks has been documented by several authors (Rock 1991, Kerrich and Wyman 1994, Armstrong and Barnett 2003, Ayer and Wyman 2003, Štemprok and Seifert 2011, Zuo *et al.* 2011, Ibrahim *et al.* 2015) in spatial and temporal associations, such as in porphyry deposits (Seedorff *et al.* 2005), diamond in the primary source (Lefebvre *et al.* 2005), and orogenic gold (mesothermal) (Taylor *et al.* 1994, Craw *et al.* 2006). Lamprophyric rocks, according to Rock (1991), are separated in to five groups as follows: alkaline, calc-alkaline and ultramafic lamprophyres, lamproites, and kimberlites, although the last two are not considered to be lamprophyric rocks anymore (Le Maitre 2002), since they are best considered independently. Calc-alkaline lamprophyres, namely, minettes, kersantites, spessartites, and vogesites, are usually found in convergent settings (Rock 1991,

Krmíek and Rao 2022), associated with calc-alkaline granitoid plutons, where they are the mafic members of dyke suites and with shoshonitic suites. The more typical association is with late- to post-orogenic bodies, including ring complexes (Rock 1991). Alkaline and ultramafic lamprophyres are commonly related to divergent environments (Krmíek and Rao 2022), with alkaline lamprophyres occurrence associated with alkaline syenite-gabbro plutons or unrelated to other igneous activity, and ultramafic lamprophyres associated with alkaline complexes (Rock 1991).

From a petrological point of view and in terms of classification, the lamprophyres are a group of meso to melanocratic rocks, usually hypabyssal, exhibiting a remarkable panidiomorphic texture, with abundance in mafic phenocrysts of biotite/phlogopite and/or amphibole, with or without pyroxene and olivine, surrounded by a matrix made up of the same mineral phases, with the addition of feldspars and/or feldspathoids (Streckeisen 1979, Le Maitre 1989). In the case of spessartite lamprophyres, they would be characterized by a felsic mineralogy (predominantly in the matrix) constituted by plagioclase >> K-feldspars and a mafic mineralogy (phenocrysts and matrix) represented mainly by hornblende >> augite.

Studies concerning the physical properties of lamprophyric rocks (*sensu* Le Maitre 2002) in the literature are rare (e.g., Rao 2008, Nishad *et al.* 2013, Hroudá *et al.* 2016), while studies applying geophysical techniques are almost non-existent (e.g., Macheck *et al.* 2014). Considering the relationship between lamprophyres and some types of ore deposits and the frequent use of gamma spectrometric, magnetometric,

Supplementary data

Supplementary data associated with this article can be found in the online version (<http://sfbjg.siteoficial.ws/Sf/2022/488920220210051.pdf>).

¹Programa de Pós-Graduação em Geociências, Instituto de Geociências, Universidade Federal do Rio Grande do Sul – Porto Alegre (RS), Brazil. E-mails: andersonbaesso96@gmail.com, carlos.sommer@ufrgs.br, jairo.savian@ufrgs.br, johnathanhenrique@hotmail.com, robgeo@ig.com.br

*Corresponding author.



and gravimetric surveys in the early stages of prospection, this work provides results that can be useful in exploration.

In the Sul-Riograndense Shield (SRGS), spessartitic (calc-alkaline) lamprophyres can be found among the lithotypes that compose the Camaquã Basin (CB) and their occurrence is linked to the Neoproterozoic Hilário Formation (Ribeiro and Fantinel 1978) of the Lavras do Sul Shoshonitic Association (LSSA) (Nardi and Lima 1985). Au and Cu mineralizations were recorded in LSSA rocks (Carvalho 1932, Ribeiro 1966, Nardi 1984, Müller *et al.* 2012, Lopes *et al.* 2014), and gold mining has developed sporadically in the district of Lavras do Sul since the early 19th century (Grazia and Pestana 2005). Lamprophyric rocks (calc-alkaline) related to the LSSA were reported as host rocks of Cu mineralization on an abandoned mine by Lopes *et al.* (2014). Müller *et al.* (2012) suggest that a possible mixture between latitic and lamprophyric magmas may have generated the ideal conditions for Au transport and precipitation in the latitic dikes of LSSA. However, the geophysical studies in south Brazil have been developed in regional scale (e.g., Costa *et al.* 1995, Fernandes *et al.* 1995, Hartmann *et al.* 2016a, 2016b), while to delimitate the bodies of this important region is less investigated, and its mineral potential under-estimated.

Geophysical techniques have been widely used in the study and mapping of igneous bodies and lavas (e.g., Blum 1945, Bott and Smithson 1967, Davis and Guilbert 1973, Grasty *et al.* 1979, Graham and Bonham-Carter 1993, Segev *et al.* 1993, Dickson and Scott 1997, De Castro 2005, Calvín *et al.* 2014, Nardy *et al.* 2014, Abedi *et al.* 2018). Gamma spectrometry surveys are a powerful tool for rock characterization because it is possible to map the radiation distribution emitted by the natural decay of K, U, and Th that can be used in the investigation of outcropping igneous rocks and related alteration (e.g., Shives *et al.* 2000, Zuzana *et al.* 2009). The gamma ray spectrometry surveys map the relative abundance or concentration of K, U, and Th in rocks and soil materials up to approximately 50 cm deep (e.g., Dickson and Scott 1997, Minty 1997, Wilford *et al.* 1997, Wilford 2002). Important information is also obtained from the element ratios (e.g., eU/eTh, eU/K, and eTh/K) and ternary K-eU-eTh radioelement maps. Magnetometry commonly shows good response to igneous bodies and has been widely used in its mapping, particularly in the prospection of primary source diamonds (kimberlitic and lamproitic bodies), especially in airborne surveys for its low cost and high sensitivity (e.g., Macnae 1995, Kono 2007). Igneous rocks, in particular, basic igneous rocks, have the highest magnetic susceptibilities due to their relatively high magnetite content and can generate significative magnetic anomalies (e.g., Geldart *et al.* 1990, Lino *et al.* 2018). Gravimetry has been used in the search and characterization of any targets that have significant density contrasts (Nabighian *et al.* 2005), which frequently is the case in igneous bodies. The technique is ideal for studying shallow subsurface geological structures related to magmatic chambers in volcanic environments (Rymer and Brown 1986, Battaglia *et al.* 2008) and can be applied to small-scale features (e.g., Breytenbach and Bosch 2011).

Detailed geophysical surveys are used to make considerations regarding the size and geometry of kimberlitic and lamproitic bodies and to identify faciological variations and

different intrusive phases (Macnae 1995). These studies allow accurate estimates of location and depth of subsurface bodies. The application of geophysical techniques to detect small igneous bodies is predominantly described for the study of kimberlitic and lamproitic pipes and diatremes, due to their economic importance, but it has also been applied to other small bodies such as dikes, plugs, and sills (Horsman *et al.* 2009).

In the northern portion of the SRGS, in the Cerro Tupanci region, an intrusive body of spessartitic lamprophyre (calc-alkaline) occurs, with fragmented texture, composed of fragments of trachyandesites and espessartites, mafic/ultramafic xenoliths, crystal fragments, mainly of amphiboles, pyroxene and plagioclasiun, and vitreous material. Secondary minerals are carbonate, chlorite, and epidote. In the matrix Fe-Cu sulphides, gold and platinum were identified using scanning electronic microprobe (Buckowski 2011). According to the author, this body is 300 m long and 40 m wide, with N-NE direction. Descriptively, this rock is classified as a lapilli tuff following the classification proposed by Gillespie and Styles (1999). In this study, we propose to accomplish a geophysical characterization using magnetometry, gamma spectrometry, and gravimetry and model this intrusive body in order to better define its dimensions and form. Magnetic susceptibility and density data are also described.

GEOLOGICAL SETTING

The Neoproterozoic to Ordovician CB is a molassic basin associated with the late to post-collisional phases of the Dom Feliciano Belt of Brasileiro Cycle (Fragoso-Cesar *et al.* 1984, Paim *et al.* 2000, Hartmann *et al.* 2008). According to Paim *et al.* (2014), the CB keeps the record of four basins overlap: Maricá foreland basin, Bom Jardim west and east strike-slip basins, Santa Bárbara west and east rifts, and Guaritas rift. Volcanic events occurred concomitantly with sediment deposition at least in three of these basins: Hilário volcanism in the Bom Jardim west and east strike-slip basins, Acampamento Velho volcanism in the Santa Bárbara west and east rifts basins, and Rodeio Velho volcanism in the Guaritas rift basin (Lima *et al.* 2007, Paim *et al.* 2014).

Hilário volcanism represents the first major magmatic episode of CB (Wildner *et al.* 2002, Lima *et al.* 2007, Sommer *et al.* 2011). The volcanic rocks of Hilário Fm. predominantly have intermediate composition, but vary from basic to acidic, with shoshonitic affinity (Nardi and Lima 1985, Lima 1995, Nardi and Lima 2000, Almeida *et al.* 2012). The effusive rocks are mainly represented by trachybasalts and trachyandesites, associated with monzonitic, quartz-monzonitic, and lamprophyric hypabissal rocks (Lima *et al.* 2007), in addition to the occurrence of volcanoclastic deposits such as breccias and tuffs. Janikian *et al.* (2008) obtained U-Pb and Ar-Ar ages from 585 to 590 My in andesites. U-Pb dating in SHRIMP from andesite zircon grains indicated ages of 580 ± 3.6 My (Janikian *et al.* 2012), and dating performed on lamprophyres by Almeida *et al.* (2012) using the U-Pb method resulted in ages of 591.8 ± 3 My. The Hilário Fm. rocks are genetically linked to the LSSA magmatism and represent its volcanic manifestation (Nardi and Lima 1985, Lima *et al.* 2007), while the plutonic phase

is represented by the nucleus of the Lavras do Sul Granitic Complex (LSGC; Nardi 1984) and consists of monzogranitic and granodioritic intrusives.

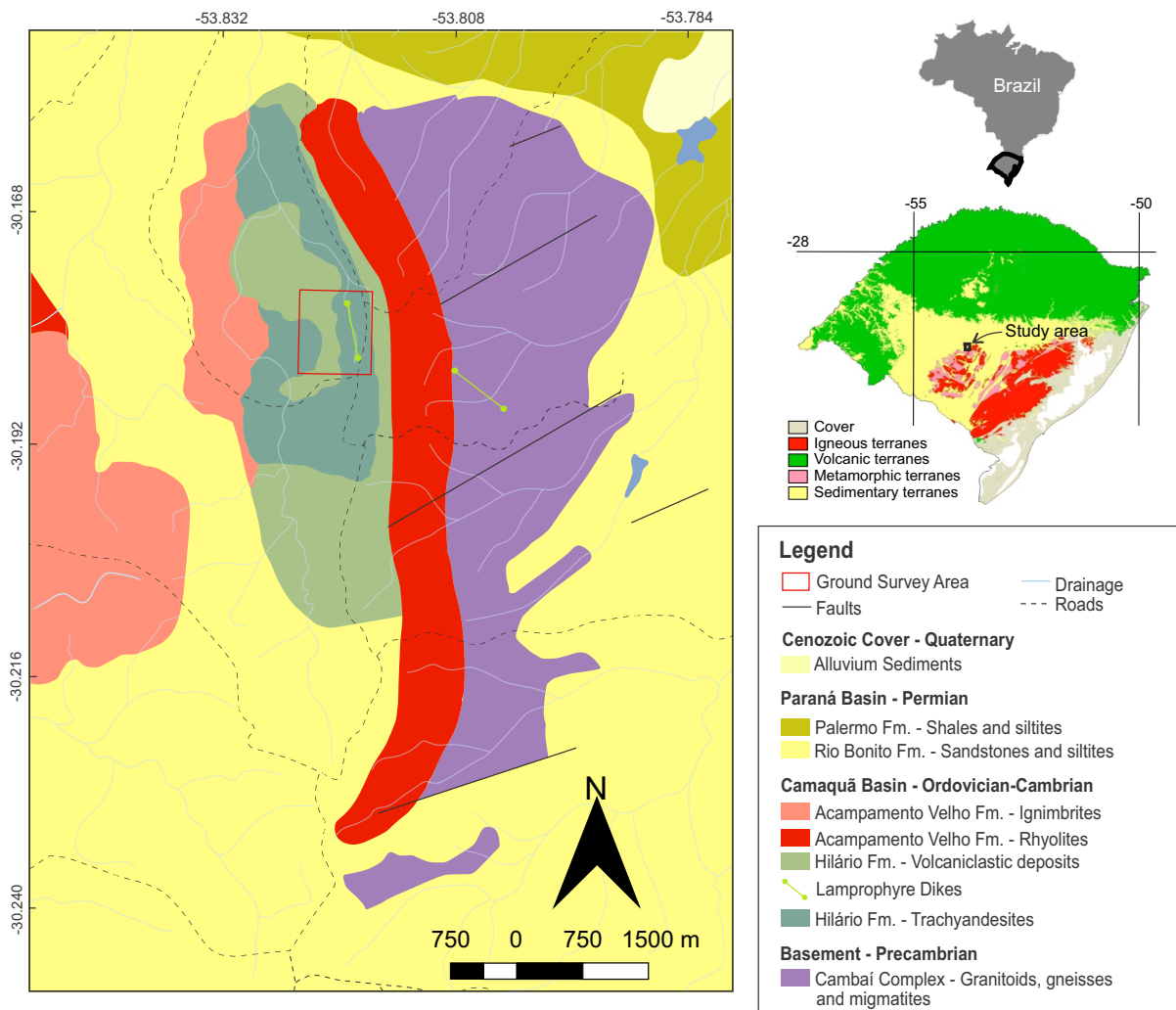
The geology of the Cerro Tupanci region is represented by trachyandesites, lamprophyres, and volcaniclastic deposits of Hilário Formation, as well as rhyolites and ignimbrites of Acampamento Velho Formation (Fig. 1). The basement is represented by granites, gneisses, and migmatites of the Cambaí Complex (Menegotto and Medeiros 1976, Buckowski 2011, Leitzke 2011, 2013, Barrios 2015). These units are covered by sedimentary rocks of Rio Bonito Formation of the Paraná Basin.

The study dike of lamprophyre is intrusive in the trachyandesitic rocks and has an average thickness of 40 m, elongated in the N-NE direction (Fig. 1). It presents a brecciated texture, with andesite and lamprophyre fragments and macrocryst fragments of clinopyroxene and amphibole surrounded by a matrix containing plagioclase, clinopyroxene, and amphibole fragments, being classified as a lapilli tuff with spessartitic composition (Buckowski 2011). The matrix is quite altered, mainly to carbonates, chlorite, and epidote. In the region, there is also a massive lamprophyric dike, intrusive in the Cambaí Complex granitoids.

MATERIAL AND METHODS

The geophysical data used in this study were obtained in a field campaign in study areas where the lamprophyric lapilli tuff outcrops (Fig. 2). Regular measurements were taken in 60 geophysical stations spaced 50 m, arranged in four N-S profiles (Fig. 3A). Gamma spectrometry, gravimetry, and magnetometry data were measured in all geophysical stations. A TopCon Hyper Lite model geodetic GPS with 3 mm horizontal and 5 mm vertical accuracy was used to determine the geographic coordinates and altitude of each point, which are fundamental in potential geophysical methods.

Gamma spectrometry measurements (K, eU, eTh) were performed at each point using a Radiation Solutions RS 125 Super Spec gamma spectrometer, where the rock was not or less weathered, in order to reduce the effects of alteration in the gamma spectrometric data. Magnetic data were collected using two proton precession magnetometers (GEM System Inc. Canada), GST 19 model with a resolution of 0.01 nT. The International Geomagnetic Reference Field (IGRF) calculated for the study area at the time of the survey showed an inclination of -38.34° , a declination of -14.22° , and an intensity of



Source: modified from Barrios (2015).

Figure 1. Location of the study area and geological map of the Cerro Tupanci region, showing the Precambrian basement, the sequences of the Camaquã Basin, and the sedimentary rocks of the Paraná Basin. The ground survey area is indicated by the red square.

21,096 nT. The gravimetric data were obtained using a Scintrex CG-3 gravimeter with a resolution of 0.005 mGal.

The geophysical data were processed using the Oasis Montaj[®] (GeoSoft) software, version 7.1.1, of Geosoft Incorporated company. Grids were interpolated using a 15-m spaced data by the minimum curvature method. For gamma spectrometry and magnetometry, we used the mean of the three measures obtained in each station. The magnetometric data were corrected for diurnal variation, and the IGRF was removed to generate a map of the local magnetic field, on which we applied filters of reduction to the magnetic pole, analytic signal, and upward continuation (UC). Reduction to the magnetic pole is a transformation of the magnetic data to the magnetic pole, intended to remove the effects of induced magnetization and strike on the shape of the anomaly (Baranov and Naudy 1964); the analytic signal is function that shift the anomaly peak to coincide either with the center or with the edges of the magnetic anomaly (Nabighian 1972); and the UC is a filter used to minimize or remove the effects of shallow sources or noise, better constraining the deeper sources. To help in the interpretation of the magnetic data, we measured the magnetic susceptibility of the outcropping rocks in the area using a MFK1-FA Multifunction Kappabridge magnetic susceptibility analyzer. The measurements were taken at the Palaeomagnetism Laboratory (USPmag), University of São Paulo, in low (976 Hz) and high (15,616 Hz) frequencies.

For gravity data, we corrected the variations caused by instrumental drift and terrain and applied free air and Bouguer reductions. To generate the Bouguer Anomaly Map, we considered a 2.67 g/cm³ density for the crust. The terrain correction applied to the gravity was made by an algorithm available on Geosoft that combines the algorithms of Kane (1962) and Nagy (1966). We collected density data from samples of different lithologies that occur in the area to better understand the sources of the gravity anomalies. The measurements were taken using liquid pycnometers, where the mass weight of the specimen divided by the volume (mass) of water displaced determines the density of the sample.

The modeling of a subsurface body from geophysical data can be carried out by the direct problem, where the physical problem is generated to calculate the response from the physical properties of rocks inside, or the inverse problem, where the physical parameters are calculated from the observed data (Barbosa and Pereira 2013). Part of the magnetometric data was selected to generate a 3D model by inversion using a 3D voxel-based algorithm available on Geosoft. A linear trend surface was removed from these data, and an Iterative Reweighting Inversion (IRT) link was used, which improves the geometry of the model focusing on the body, making it less dispersed (Barbosa and Pereira 2013). Using the gravimetric data, we generated a model by the direct (or forward) method in a profile of orientation E-W, crosscutting the body, using the GM-SYS integrated with the OMG platform.

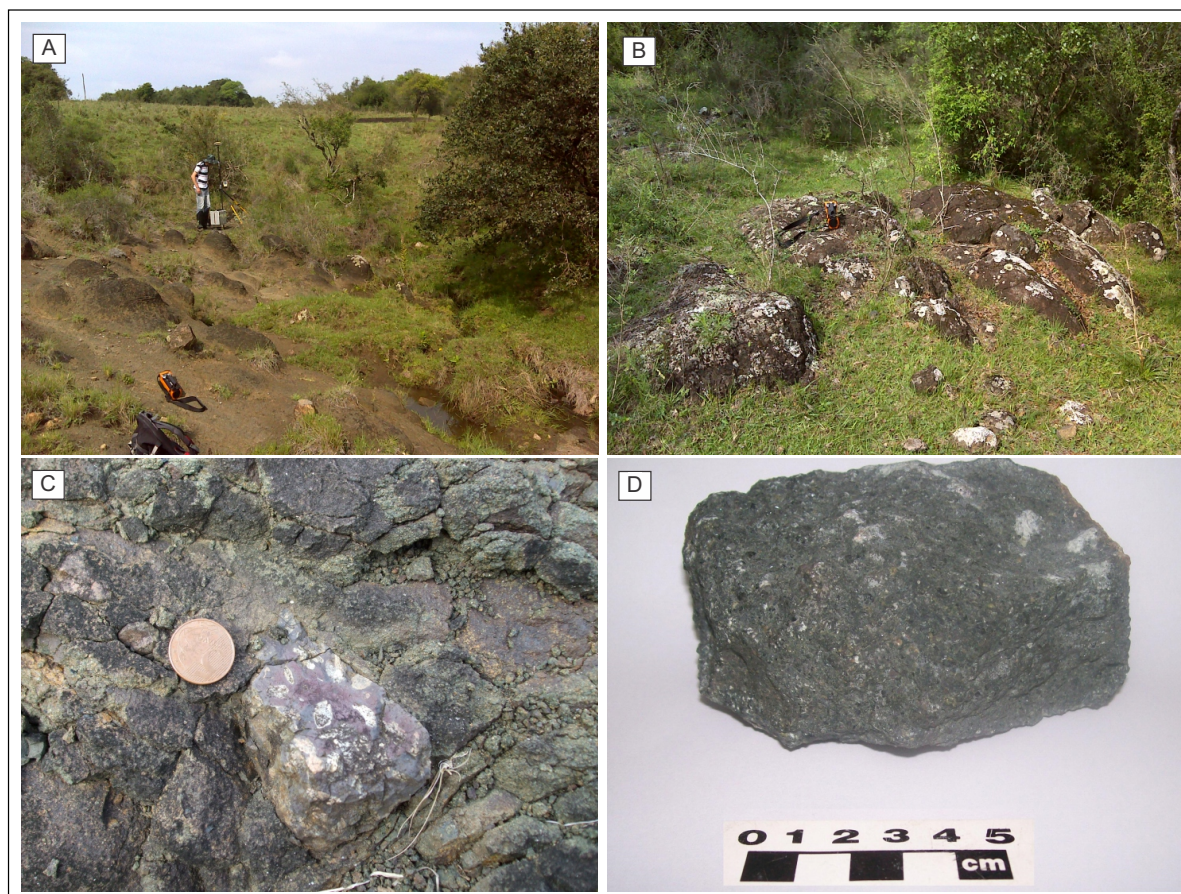


Figure 2. (A and B) Photographs of two areas showing the lapilli tuff outcrops. (C) An accidental fragment of andesite immersed in the lapilli tuff. (D) A sample used to obtain the density and magnetic susceptibility data.

RESULTS AND DISCUSSION

The lapilli tuff is constituted by accidental fragments of andesites and cognate fragments of a lamprophyric rock engulfed by a tufaceous matrix (Buckowski 2011). In the field, a massive rock was observed (Figs. 2A and 2B), with a particulate texture (Figs. 2C and 2D), locally occurring spherical

exfoliation (Fig. 2A). The lapilli tuff outcrops in the bottom of a small stream and in the surrounding areas.

Petrophysical data

Table 1 shows the density and magnetic susceptibility data obtained for different rocks from the study area. The measured

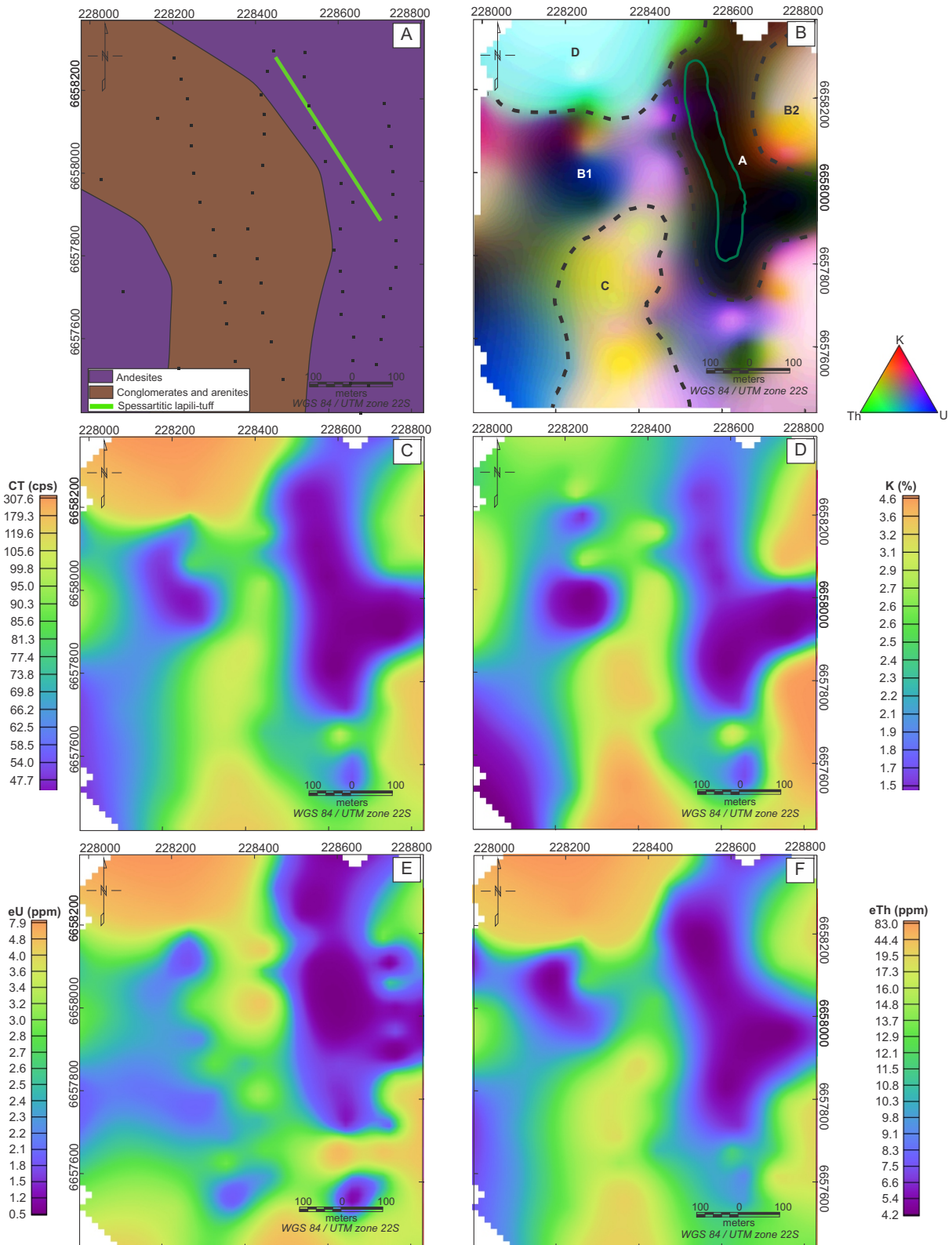


Figure 3. (A) Location of the measurement places for the geophysical data (black dots) on the geological map of Barrios (2015). (B) Ternary map (red-green-blue colors) of the study area, area of the outcropping lamprophyre, and radiometric domains. (C–F) Total counts, potassium, uranium, and thorium maps for the area, respectively. All maps indicate an anomaly with low values in the approximate location of the lamprophyre.

density of the sampled rocks varies between 2.26 g/cm³ for the arenite and 2.91 g/cm³ for the lamprophyre. The obtained density for the lamprophyre is consistent with data published on New Zealand lamprophyres by Tenzer *et al.* (2011), with density values between 2.65 and 3.39 g/cm³. The magnetic susceptibility obtained from the lamprophyre sample showed positive values (1.28×10^{-6} S.I.), indicating a paramagnetic behavior (Clark 1999).

Gamma spectrometry

The radiometric ternary map of RGB (red, green, blue) composition of potassium (K), equivalent thorium (eTh), and equivalent uranium (eU) elements was generated (Fig. 3). It was possible to divide the study area into five radiometric domains: A, B1, B2, C, and D. Radiometric domain A covers an area approximately coincident with the outcropping area of the lapilli tuff. It has low total count, K, eU, and eTh, respectively, 30–54.7 counts per second (cps), 0.8–2%, 0.4–1.9 ppm, and 4–7 ppm. The radiometric domain B1 and B2 corresponds approximately to the areas where trachyandesites outcrop. It has intermediate to high values for total count (50–150 cps) and widely varying values for K (1.3–4%), eU (1.6–5.3 ppm), and eTh (6–18 ppm). The domain C is located in the southern part of the study area, where conglomerates and sandstones outcrop. The total count, K, and eTh values are high (80–130 cps, 2.8–4.4%, and 12–30 ppm, respectively). Equivalent uranium values are moderate (1.9–2.8 ppm). The radiometric domain D is in the northwestern portion of the study area and also corresponds to trachyandesites. These have high values for total count (90–260 cps), eU (3–6.7 ppm), and eTh (20–70 ppm), and moderate K values (2–2.8 ppm).

The contrast of K, eU, and eTh between domains A and B reflects the compositional variation between lamprophyre and trachyandesites. However, at two points, east of the intrusive body, occur sandstones whose values of these elements do not differ from the lapilli tuff so that these two lithologies are grouped into the same domain (i.e., domain A).

The domain D, although occurring in an area where the outcropping lithology is trachyandesite, has very high eU and eTh values, totally different from the values obtained in other areas of the same lithology. A macroscopic analysis of the domain D trachyandesites showed that the feldspar phenocrysts are strongly altered for epidote and clay minerals. The cause of these higher values can be related to the passage of hydrothermal fluids altering the rock and causing uranium and, particularly, thorium enrichment. It is also important to note that this domain's area is unlikely to be true to the field occurrence of hydrothermalized trachyandesites, since the measurement stations with these values are at the edge of the map, and when interpolated by minimal curvature, surface smoothing must have extrapolated these high values to a larger area than the actual one. In fact, these anomalous values were obtained at only three measurement stations.

Thorium enrichment in hydrothermal environments can generate one of the four main types of deposits of this element, which are deposits in veins (Barthel and Tulsidas 2014). According to the authors, vein deposits occur in or close to intrusive or extrusive igneous rocks. The enrichment observed in hydrothermalized trachyandesites may have a similar origin, although less intense. In addition, studies in the lamprophyric rocks of this region (Buckowski 2011) show a concentration of K₂O, U, and Th varying from 0.76 to 1.39%, 1.1 to 2.0 ppm, and 3.52 to 4.9 ppm, respectively, while the trachyandesitic host rocks show concentrations of K₂O from 2.7 to 6.4%, U from 1.2 to 4.8 ppm, and Th from 5.1 to 15.2 ppm (Barrios 2015).

Magnetometry

Figure 4 shows the total magnetic field map reduced from IGRF to the area. The reduction to pole (RTP), analytic signal amplitude (ASA), and UC filters were applied to these data and are shown in the same figure.

In the area, the magnetic field has a magnitude of about 190 nT, with higher values predominantly in the south and lower

Table 1. Density and magnetic susceptibility data for some rocks of the Cerro Tupanci region*.

Sample ID	Lithology	Field (A/m)	Frequency (Hz)	Mass (g)	Susceptibility (S.I. units)	Density (g/cm ³)
CTG092	Siltite	200	15,616	20.069	1.75×10^{-7}	2.68
CTG039	Conglomerate	200	15,616	23.371	3.39×10^{-8}	2.62
CTG072	Arenite	200	15,616	20.243	-5.62×10^{-9}	2.26
CTG079	Ignimbrite	200	15,616	22.545	3.40×10^{-8}	2.46
CT74	Lamprophyre	200	15,616	21.032	1.28×10^{-6}	2.91
CTG086	Riolite	200	15,616	29.6	1.50×10^{-6}	2.50
CT09F	Trachyandesite	200	15,616	22.351	1.19×10^{-5}	2.74
CTG092	Siltite	200	976	20.069	2.03×10^{-7}	
CTG039	Conglomerate	200	976	23.371	3.88×10^{-8}	
CTG072	Arenite	200	976	20.243	-3.47×10^{-9}	
CTG079	Ignimbrite	200	976	22.545	4.05×10^{-8}	
CT74	Lamprophyre	200	976	21.032	1.30×10^{-6}	
CTG086	Riolite	200	976	29.6	1.52×10^{-6}	
CT09F	Trachyandesite	200	976	22.351	1.20×10^{-5}	

*The magnetic susceptibility for the igneous rocks is similar, except for the ignimbrites.

values in the east and north portions, with an anomaly characterized by a dipole in the north-central part of the study area. This anomaly is not centered over the lapilli tuff, but slightly to the west. From the RTP map (Fig. 4), two magnetic domains and the anomaly were separated. Magnetic domain A presents intermediate to low values, ranging from -34 to 73 nT, and occupies the north and east edges of the map, practically surrounding the magnetic dipole. Magnetic domain B is located in the south-west part of the map and covers a large area, with a northwest direction boundary with dipole and domain A. It has magnetic field values higher than domain A, ranging from 73 to 155 nT.

The dipole is located in the central and northern parts of the map (Fig. 4A). The source area is estimated from a circle whose edges run over the center of the two poles, resulting in an area of about 4 ha. It presents normal polarization for the southern hemisphere, with minimum values of -43 nT and maximum values of 129 nT. The magnetic data inversion in the dipole area was performed to obtain a model of its causative body. Thus, a three-dimensional magnetic susceptibility

distribution model was created (Fig. 5A). Figures 5B and 5C shows sections on the Y- and X-axes, respectively, and Fig. 5D shows a section on magnetic susceptibility values. From the generated model, it is observed that this anomaly presents its upper limit at approximately 105 m over the sea level, i.e., about 70 m deep, with a cylindrical shape.

The absence of an anomaly linked to the lamprophyric body is coherent with the magnetic susceptibility data obtained for this rock type (1.28×10^{-6} S.I.), which is not much different than the values obtained for the other igneous rocks present in the area (1.50×10^{-6} S.I. for rhyolites and 1.19×10^{-5} for trachyandesites).

Gravimetry

Figure 6 shows the Bouguer Anomaly Map of the area. Four gravimetric domains were divided into domains A, B, C, and D. The gravimetric domain A corresponds approximately to the area where the lapilli tuff emerges. It is characterized by a negative anomaly, elongated in the N-S direction, with values between -20 and -18 mGal. Gravimetric domain B occupies

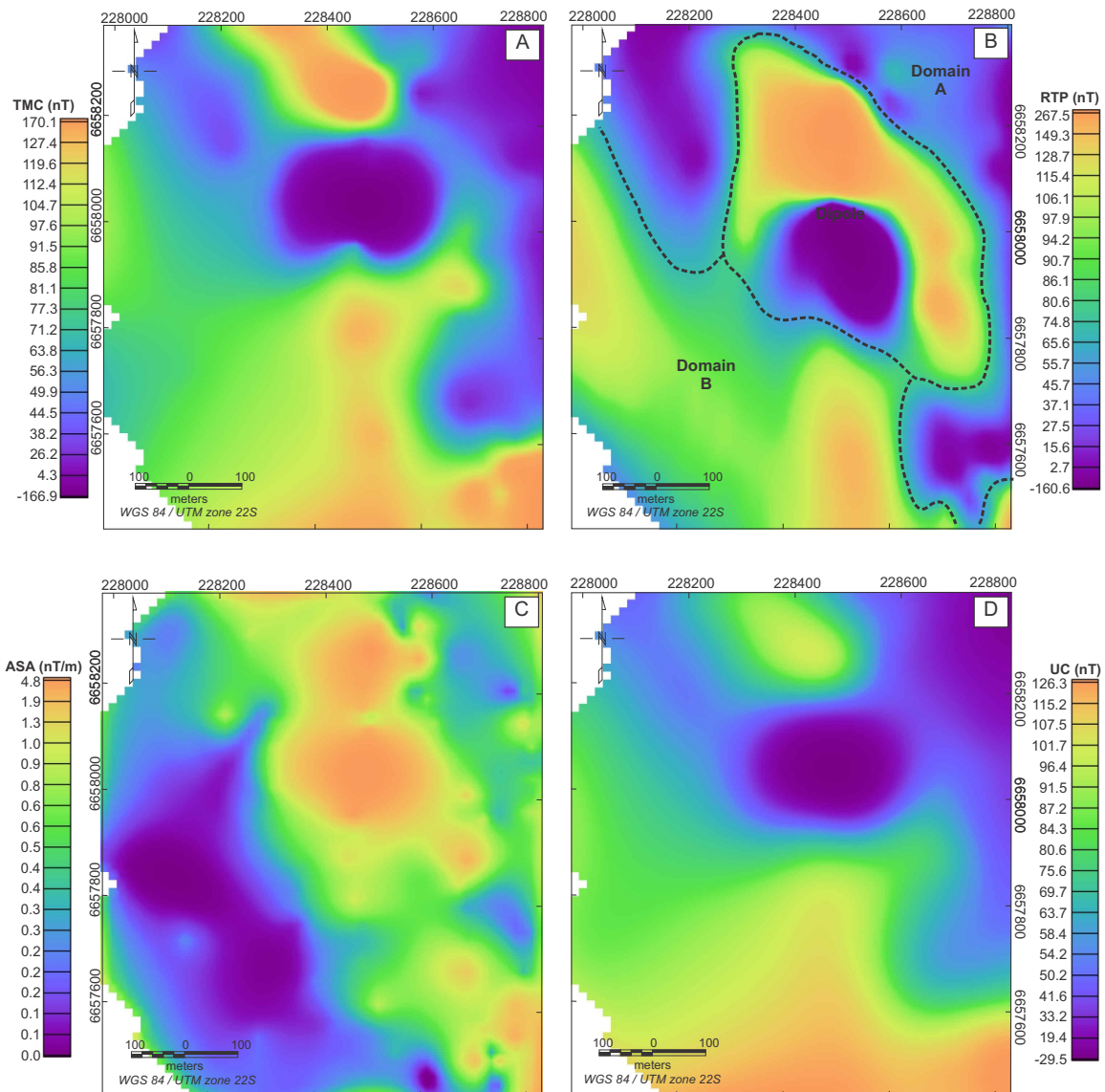


Figure 4. (A) Total magnetic field map reduced from IGRF showing a dipole in the northern portion. (B) Total magnetic field reduced to the magnetic pole showing the dipole and domains A and B. (C and D) The analytical signal and upward continuation (50 m) maps, respectively.

a small area west of domain A, with low Bouguer anomaly values between -19 and -18 mGal. The gravimetric domain C occupies the entire southwest area of the map, with moderate to high Bouguer anomaly values between -15 and -18 mGal. The gravimetric domain D occupies the eastern edge of the study area and has high values of gravity, predominantly higher than -16.5 mGal, reaching the highest values obtained in the area, up to -14 mGal. For the gamma spectrometric, magnetic, and gravimetric field data, refer to Supplementary material.

Using the direct problem, the subsurface geology was modeled in an east-west profile, perpendicular to the dike. The modeled profile is shown in Fig. 7. For the construction of the model, the density of the trachyandesites was obtained from field samples and their surface boundaries were also determined in the field. The basement was assumed to be the Cambaí Complex, which occurs adjacent to the area and is formed by gneisses in this region. Densities of this rock type range from 2.6 to 2.9 g/cm³ (Sharma 1997), and we have chosen the value that, within this range, best approximated the calculated gravity to that observed. The density of lapilli tuff was chosen from values presented for densities of pyroclastic and epiclastic rocks of kimberlitic composition, whose lowest values reach 1.8 g/cm³ (Arnott and Kostlin 2003). The non-outcropping body geometry was copied from the model generated by the inversion of the magnetic data. Its density, as well as the boundary between trachyandesites and basement, was chosen to best fit the calculated gravity with the observed gravity.

The Bouguer Anomaly Map has a clear negative anomaly coincident with the outcropping area of the lapilli tuff. According to Parasnis (1973), deep bodies cause large anomalies with low amplitudes, while shallow bodies generate restricted and clear anomalies. Thus, apparently, the lapilli tuff generates a negative anomaly where it is found. However, analyses of samples of lapilli tuff resulted in a density of 2.93 g/cm³, higher than the density of the host rocks (trachyandesites: 2.73 g/cm³; conglomerates: 2.6 g/cm³). Considering that the lapilli tuff is a rock with fragmented texture from which were chosen the less altered samples, and is located a few kilometers from where the basement of the CB emerges, the following possibilities were raised:

- Density measurements do not correspond to reality since samples were chosen from the less fractured and hydrothermalized parts, and the actual density of lamprophyres is lower than that of the host rocks. Densities of the crater facies of kimberlites (pyroclastic and epiclastic, most similar to the texture of the lapilli tuff) are low, reaching 1.8 g/cm³ (Arnott and Kostlin 2003). Densities of pyroclastic rocks of New Zealand vary between 1.13 and 2.35 g/cm³ (Tenzer *et al.* 2011);
- In the area where occurs the lamprophyre, the CB exposition is thin, and the basement (Cambaí Complex) is just a few meters below. If the basement is denser than the lapilli tuff, it could explain the negative anomaly.

It is also possible that both hypotheses are true, with lamprophyre density lower than that measured in the laboratory and a shallow basement, denser than the lapilli tuff. The model

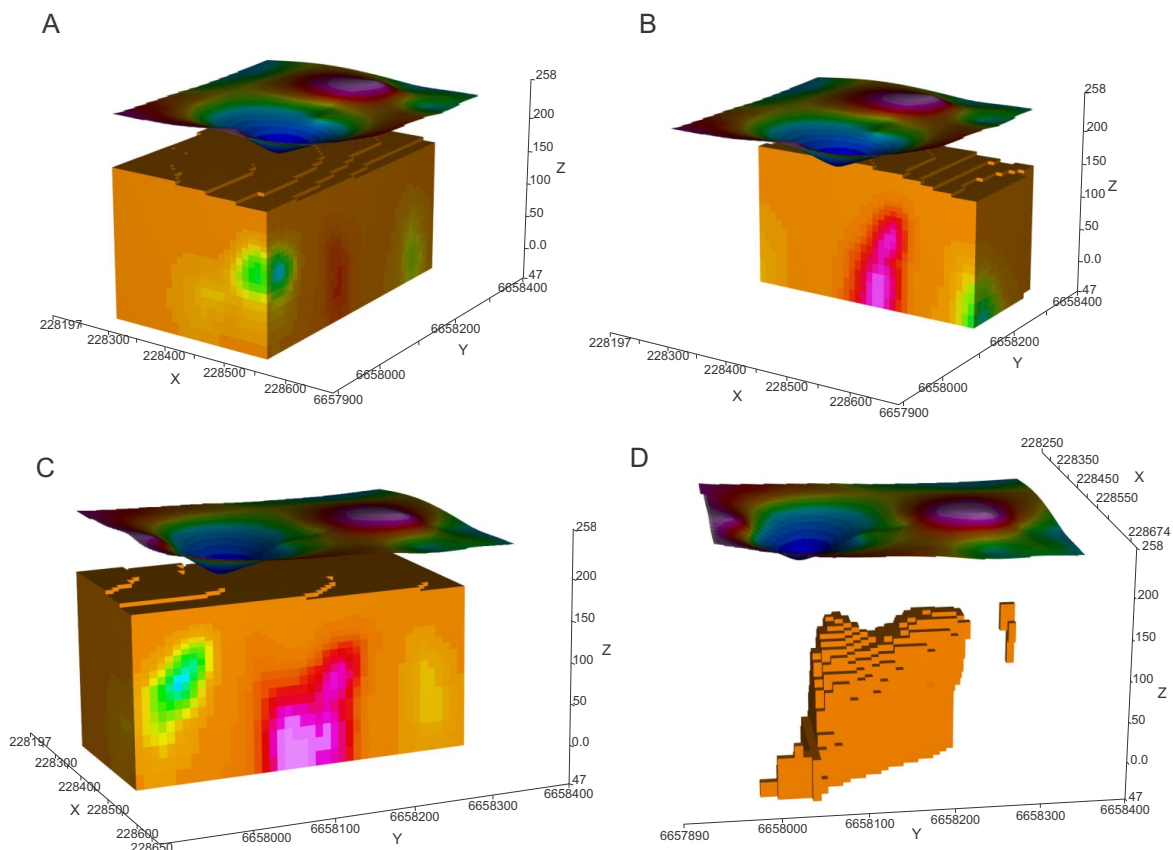


Figure 5. Magnetic susceptibility model of the subsurface generated from the magnetic data. (A) Area of the magnetic anomaly and the model. (B and C) Sections on the Y- and X-axes, respectively. (D) A cut in the lowest magnetic susceptibility values.

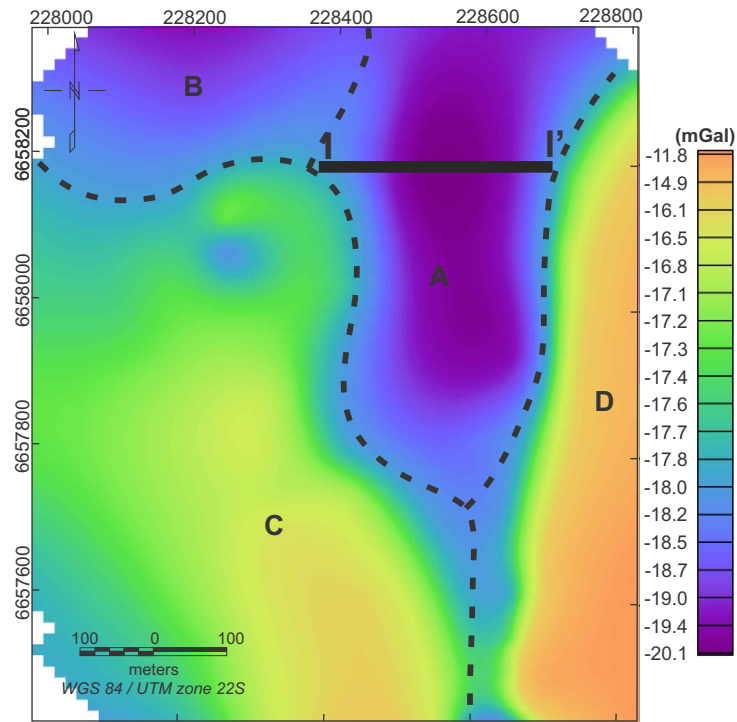
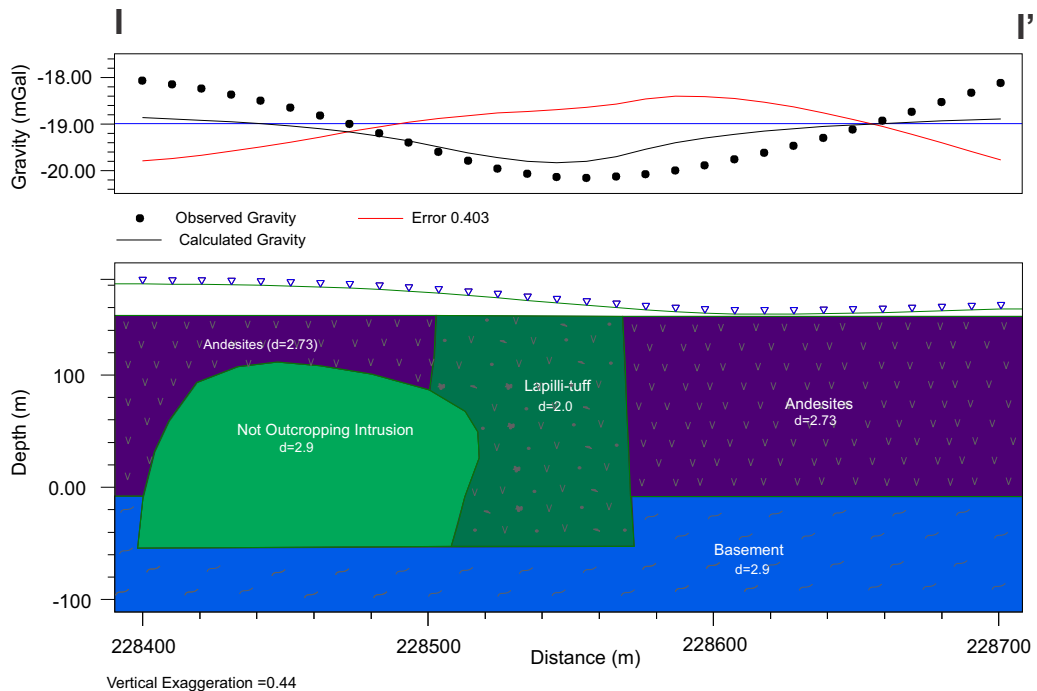


Figure 6. Bouguer Anomaly Map for the study area and gravimetric domains. Profile I – I' corresponds to the 2D gravity model.



d: density.

Figure 7. 2D model generated from the gravimetric data. The not outcropping intrusion is the possible intrusive body suggested by the magnetometric data.

generated from the gravimetric data allowed a reasonable fit between the measured and observed gravity. The near-surface dike boundaries were established according to the observed field geology. The largest error in the fit between the calculated and observed data occurs slightly west of the dike, where, to satisfy the gravimetric data, it would have a larger extent,

with nearly twice the observed surface width. This difference between geology and geophysics may be caused by interpolation of the field data, which may have made the anomaly larger than it really is in the east-west direction.

Another remarkable fact is that there is no gravity anomaly corresponding to the magnetic anomaly. Assuming the

existence of the intrusive body mentioned in the discussion of magnetic data, its density should be higher than that of the lapilli tuff and very similar to that of the surrounding rocks, i.e., about 2.6–2.8 g/cm³. To better characterize the subsurface of the area, other evaluation methods (e.g., drilling) are necessary.

CONCLUSIONS

The gamma spectrometric and gravimetric data obtained in the field have shown a clear response to the lamprophyre body. An anomaly with low values of total counts, K, eU, and eTh occurs in the area where the lamprophyre outcrops, as well as a negative Bouguer anomaly. These anomalies have approximately 450 m length and 70 m width in the N-S direction. The

magnetic data showed no response to the lamprophyre dike but presented a dipolar anomaly, suggesting the existence of a small intrusive with distinct magnetic susceptibility in the area.

ACKNOWLEDGMENTS

This study was partial financed by CNPq (C. A. Sommer — 304036/2018-8, 406925/2018-6) and Instituto de Geociências, Universidade Federal do Rio Grande do Sul. Anderson Baesso thanks the Coordenação de Aperfeiçoamento de Pessoal de Nível Superior — Brasil (CAPES) for research grant. We also thank the Companhia de Pesquisa de Recursos Minerais (CPRM) for lending us the magnetometers. At last, we thank the Laboratório de Paleomagnetismo of the Universidade de São Paulo.

ARTICLE INFORMATION

Manuscript ID: 20210051. Received on: 29 JUN 2021. Approved on: 16 MAY 2022.

How to cite this article: Baesso A., Sommer C.A., Savian J.F., Gambeta J.H., Aquino R.D.S. Neoproterozoic intrusive volcanoclastic lamprophyre in the southernmost Brazil: geophysical characterization and modeling. *Brazilian Journal of Geology*, 52(3):e20210051, 2022. <http://sfbjg.siteoficial.ws/Sf/2022/4889202220210051.pdf>.

A.B.: conceptualization, data curation, methodology, writing — original draft, writing — review & editing. C.A.S.: Conceptualization, data curation, funding acquisition, methodology, writing — review & editing. J.F.S.: Conceptualization, data curation, methodology, software, writing — review & editing. Johnathan H. Gambeta: Data curation, writing — review & editing. R.D.S.A.: Data curation, methodology.

Competing interests: The authors declare no competing interests.

REFERENCES

- Abedi M., Fournier D., Devriese S.G.R., Oldenburg D.W. 2018. Integrated inversion of airborne geophysics over a structural geological unit: A case study for delineation of a porphyry copper zone in Iran. *Journal of Applied Geophysics*, 152:188-202. <https://doi.org/10.1016/j.jappgeo.2018.04.001>
- Almeida D. del P.M., Chemale F., Machado A. 2012. Late to Post-Orogenic Brasiliano-Pan-African Volcano-Sedimentary Basins in the Dom Feliciano Belt, Southernmost Brazil. *Petrology - New Perspectives and Applications*, 5:73-105. <https://doi.org/10.5772/25189>
- Armstrong J., Barnett, R. 2003. The association of Zn-chromite with diamondiferous lamprophyres and diamonds: unique compositions as a guide to the diamond potential of non-traditional diamond host rocks. In: International Kimberlite Conference. *Extended Abstracts...*, 8. <https://doi.org/10.29173/ikc3143>
- Arnott F., Kostlin E. 2003. Petrophysics of kimberlites. In: International Kimberlite Conference. *Extended Abstracts...*, 8. <https://doi.org/10.29173/ikc3246>
- Ayer J.A., Wyman D.A. 2003. Origin of Diamondiferous Archean Lamprophyres in the evolution of the Michipicoten and Abitibi Greenstone Belts. In: International Kimberlite Conference. *Extended Abstracts...*, 8. <https://doi.org/10.29173/ikc3190>
- Baranov V., Naudy H. 1964. Numerical calculation of the formula of reduction to the magnetic pole. *Geophysics*, 29(1):67-79. <https://doi.org/10.1190/1.1439334>
- Barbosa R.D., Pereira J.G. 2013. Inversão 3D de dados magnéticos na região de Mara Rosa - Goiás, Brasil, utilizando Geosoft VOXI 520–525. In: International Congress of the Brazilian Geophysical Society & EXPOGEEF, 13., Rio de Janeiro. *Annals...* <https://doi.org/10.1190/sbgf2013-109>
- Barrios M.F.S. 2015. Geologia e petrografia das rochas andesíticas da região do Cerro Tupanci, Vila Nova do Sul, RS. Graduation Thesis, Universidade Federal do Rio Grande do Sul, Porto Alegre, 80 p.
- Barthel F., Tulsidas H. 2014. Thorium: geology, occurrence, deposits and resources. In: International Symposium on Uranium Raw Material for the Nuclear Fuel Cycle: Exploration, Mining, Production, Supply and Demand, Economics and Environmental Issues (URAM 2014), Vienna. *Proceedings...*
- Battaglia M., Gottsmann J., Carbone D., Fernández J. 2008. 4D volcano gravimetry. *Geophysics*, 73(6):WA3-WA18. <https://doi.org/10.1190/1.2977792>
- Blum V. 1945. The magnetic field over igneous pipes. *Geophysics*, 10(3):368-375. <https://doi.org/10.1190/1.1437180>
- Bott M.H.P., Smithson S.B. 1967. Gravity investigations of subsurface shape and mass distributions of granite batholiths. *Geological Society of America Bulletin*, 78(7):859-878. [https://doi.org/10.1130/0016-7606\(1967\)78\[859:GIOSSA\]2.0.CO;2](https://doi.org/10.1130/0016-7606(1967)78[859:GIOSSA]2.0.CO;2)
- Breytenbach I.J., Bosch P.J.A. 2011. Applications, advantages and limitations of high-density gravimetric surveys compared with three-dimensional geological modelling in dolomite stability investigations. *Journal of South African Institution of Civil Engineering*, 53(2):7-13.
- Buckowski N. 2011. *Caracterização dos lamprófiros espessartíticos da região de Vila Nova do Sul*, RS. Graduation Thesis, Universidade Federal do Rio Grande do Sul, Porto Alegre, 77 p.
- Calvin P., Casas A.M., Villalain J.J., Tierz P. 2014. Reverse magnetic anomaly controlled by Permian igneous rocks in the Iberian Chain (N Spain). *Geologica Acta*, 12(3):193-207. <https://doi.org/10.1344/GeologicaActa2014.12.3.2>
- Carvalho P.E. 1932. Reconhecimento Geológico no Estado do Rio Grande do Sul. *Boletim do Serviço Geológico e Mineralógico do Brasil*, 66:72.
- Clark D.A. 1999. Magnetic petrology of igneous intrusions: Implications for exploration and magnetic interpretation. *Exploration Geophysics*, 30(1-2):5-26. <https://doi.org/10.1071/EG999005>

- Costa A.F.U., Fernandes L.A.D., Shukowsky W., Nardi L.V.S., Bitencourt M. de F. 1995. Teste dos modelos tectônicos e de posicionamento do Complexo Granítico de Caçapava do Sul através de estudos de modelagem gravimétrica 3-D. *Revista Brasileira de Geofísica*, **13**(2):91-101. <https://doi.org/10.22564/rbgfv13i2.1185>
- Craw D., Begbie M., MacKenzie D. 2006. Structural controls on tertiary orogenic gold mineralization during initiation of a mountain belt, New Zealand. *Mineralium Deposita*, **41**(7):645-659. <https://doi.org/10.1007/s00126-006-0088-0>
- Davis J.D., Guilbert J.M. 1973. Distribution of the radioelements potassium, uranium, and thorium in selected porphyry copper deposits. *Economic Geology*, **68**(2):145-160. <https://doi.org/10.2113/gsecongeo.68.2.145>
- De Castro D.L. 2005. Modelagem gravimétrica 3-D de corpos graníticos e bacias sedimentares com embasamento estrutural de densidade variável. *Revista Brasileira de Geofísica*, **23**(3):295-308. <https://doi.org/10.1590/s0102-261x2005000300008>
- Dickson B.L., Scott K.M. 1997. Interpretation of aerial gamma-ray surveys - adding the geochemical factors. *AGSO Journal of Australian Geology and Geophysics*, **17**(2):187-200.
- Fernandes L.A.D., Menegat R., Costa A.F.U., Koester E., Porcher C.C., Tommasi A., Kraemer G., Ramgrab G.E., Camozzato E. 1995. Evolução tectônica do Cinturão Dom Feliciano no escudo sul-rio-grandense: parte ii - uma contribuição a partir das assinaturas geofísicas. *Revista Brasileira de Geociências*, **25**(4):375-384. <https://doi.org/10.25249/0375-7536.1995375384>
- Fragoso-Cesar A.R.S., Lavina E.L., Paim P.S.G., Faccini U.F. 1984. A antefossa molássica do Cinturão Dom Feliciano no escudo do Rio Grande do Sul. In: Congresso Brasileiro de Geologia, 33., Rio de Janeiro. *Anais... SBG*, p. 3272-3283.
- Geldart L.P., Sheriff R.E., Telford W.M. 1990. Magnetic methods. In: Geldart L.P., Sheriff R.E., Telford W.M. (Eds.). *Applied geophysics*. Cambridge: Cambridge University, p. 62-135. <https://doi.org/10.1017/CBO9781139167932.007>
- Gillespie M., Styles M.T. 1999. *BGS rock classification scheme*. Classification of igneous rocks. Nottingham. British Geological Survey Research Report, RR/08/05. v. 1.
- Graham D.F., Bonham-Carter G.F. 1993. Airborne radiometric data - A tool for reconnaissance geological mapping using a GIS. *Photogrammetric Engineering and Remote Sensing*, **59**(8):1243-1249.
- Grasty R.L., Kosanke K.L., Foote R.S. 1979. Fields of view of airborne gamma-ray detectors. *Geophysics*, **44**(8):1447-1457. <https://doi.org/10.1190/1.1441017>
- Grazia C.A., Pestana M.H.D. 2005. Contaminação por Mercúrio Antrópico em Solos e Sedimentos de Corrente de Lavras do Sul-RS-Brasil. In: International Workshop on Medical Geology, 2005, Rio de Janeiro.
- Hartmann L.A., Lopez W.R., Savian J.F. 2016a. Integrated evaluation of the geology, aerogammaspectrometry and aeromagnetometry of the Sul-Riograndense Shield, southernmost Brazil. *Anais da Academia Brasileira de Ciências*, **88**(1):75-92. <https://doi.org/10.1590/0001-3765201520140495>
- Hartmann L.A., Santos J.O.S., McNaughton N.J. 2008. Detrital zircon U-Pb age data, and Precambrian provenance of the Paleozoic Guaritas Formation, southern Brazilian shield. *International Geology Review*, **50**(4):364-374. <https://doi.org/10.2747/0020-6814.50.4.364>
- Hartmann L.A., Savian J.F., Lopes W.R. 2016b. Airborne geophysical characterization of geotectonic relationships in the southern Ribeira Belt, Luís Alves Craton, and northern Dom Feliciano Belt, Brazilian Shield. *International Geology Review*, **58**(4):471-488. <https://doi.org/10.1080/00206814.2015.1089424>
- Horsman E., Morgan S., De Saint-Blanquat M., Habert G., Nugent A., Hunter R.A., Tikoff B. 2009. Emplacement and assembly of shallow intrusions from multiple magma pulses, Henry mountains, Utah. *Earth and Environmental Science Transactions of the Royal Society of Edinburgh*, **100**(1-2):117-132. [https://doi.org/10.1130/2010.2472\(08\)](https://doi.org/10.1130/2010.2472(08))
- Hrouda F., Verner K., Kubínová Š., Buriánek D., Faryad S., Chlupáčová M., Holub F. 2016. Magnetic fabric and emplacement of dykes of lamprophyres and related rocks of the Central Bohemian Dyke Swarm (Central European Variscides). *Journal of Geosciences*, **61**(4):335-354. <https://doi.org/10.3190/jgeosci.222>
- Ibrahim M.E.A., Watanabe K., Saleh G.M., Ibrahim W.S. 2015. Abu Rusheid lamprophyre dikes, South Eastern Desert, Egypt: as physical-chemical traps for REEs, Zn, Y, U, Cu, W, and Ag. *Arabian Journal of Geosciences*, **8**(11):9261-9270. <https://doi.org/10.1007/s12517-015-1882-8>
- Janikian L., Almeida R.P., Fragoso-Cesar A.R.S., Martins V.T. de S., Dantas E.L., Tohver E., McReath I., D'Agrella-Filho M.S. 2012. Ages (U-Pb SHRIMP and LA ICPMS) and stratigraphic evolution of the Neoproterozoic volcano-sedimentary successions from the extensional Camaquã Basin, Southern Brazil. *Gondwana Research*, **21**(2-3):466-482. <https://doi.org/10.1016/j.gr.2011.04.010>
- Janikian L., Almeida R.P., Trindade R.L.F., Fragoso-Cesar A.R.S., D'Agrella-Filho M.S., Dantas E.L., Tohver E. 2008. The continental record of Ediacaran volcano-sedimentary successions in southern Brazil and their global implications. *Terra Nova*, **20**(4):259-266. <https://doi.org/10.1111/j.1365-3121.2008.00814.x>
- Kane M.F. 1962. A comprehensive system of terrain corrections using a digital computer. *Geophysics*, **27**(4):455-462. <https://doi.org/10.1190/1.1439044>
- Kerrich R., Wyman D.A. 1994. The mesothermal gold-lamprophyre association: significance for an accretionary geodynamic setting, supercontinent cycles, and metallogenic processes. *Mineralogy and Petrology*, **51**(2-4):147-172. <https://doi.org/10.1007/BF01159725>
- Kono M. 2007. Geomagnetism in perspective. In: *Treatise on Geophysics*. Amsterdam: Elsevier, 5:1-31. <https://doi.org/10.1016/B978-044452748-6.00086-9>
- Krmík L., Rao N.V.C. 2022. Lamprophyres, lamproites and related rocks as tracers to supercontinent cycles and metallogenesis. *Geological Society*, **513**(1):1-16. <https://doi.org/10.1144/SP513-2021-159>
- Lefebvre N., Kopylova M., Kivi K. 2005. Archean calc-alkaline lamprophyres of Wawa, Ontario, Canada: Unconventional diamondiferous volcanoclastic rocks. *Precambrian Research*, **138**(1-2):57-87. <https://doi.org/10.1016/j.precamres.2005.04.005>
- Leitzke F.P. 2011. *Geologia e petrologia das rochas vulcânicas ácidas da região do Tupanci, centro-oeste do RS*. Graduation Thesis, Universidade Federal do Rio Grande do Sul, Porto Alegre, 126 p.
- Leitzke F.P. 2013. *Rochas vulcânicas alta-silica na região do Tupanci, NW do Escudo Sul-Rio-Grandense*. MS Dissertation, Universidade Federal do Rio Grande do Sul, Porto Alegre, 95 p.
- Le Maitre R.W. 1989. A classification of igneous rocks and glossary of terms. Recommendations of the international union of geological sciences subcommission on the systematics of igneous rocks. New York: Cambridge University Press, 193 p.
- Le Maitre R.W. (Ed.). 2002. *Igneous rocks. A classification and glossary of terms. Recommendations of the International Union of Geological Sciences, Subcommission on the Systematics of Igneous Rocks*. New York: Cambridge University Press, 236 p. <https://doi.org/10.1017/S0016756803388028>
- Lima E.F. 1995. *Petrologia das rochas vulcânicas e hipobassais da Associação Shoshonítica de Lavras do Sul - ASLS*. PhD Thesis, Universidade Federal do Rio Grande do Sul, Porto Alegre, 338 p.
- Lima E.F., Sommer C.A., Nardi L.V.S. 2007. O vulcanismo neoproterozóico-ordoviciano no Escudo Sul-riograndense: os ciclos vulcânicos da Bacia do Camaquã. In: 50 Anos de Geologia. Instituto de Geociências. Contribuições. Porto Alegre: Comunicação e Identidade, p. 79-95.
- Lino L.M., Cavallaro F.A., Vlach S.R.D.F., Coelho D.C. 2018. 2D magnetometric modeling of a basic-intermediate intrusion geometry: geophysical and geological approaches applied to the Limeira intrusion, Paraná Magmatic Province (SP, Brazil). *Brazilian Journal of Geology*, **48**(2):305-315. <https://doi.org/10.1590/2317-4889201820180099>
- Lopes R.W., Fontana E., Mexias A.S., Gomes M.E.B., Nardi L.V.S., Renac C. 2014. Caracterização petrográfica e geoquímica da sequência magmática da Mina do Seival, Formação Hilário (Bacia do Camaquã - Neoproterozoico), Rio Grande do Sul, Brasil. *Pesquisas em Geociências*, **41**(1):51-64. <https://doi.org/10.22456/1807-9806.78035>
- Machek M., Roxerová Z., Závada P., Silva P.F., Henry B., Dědeček P., Petrovský E., Marques F.O. 2014. Intrusion of lamprophyre dyke and related deformation effects in the host rock salt: A case study from the Loulé diapir, Portugal. *Tectonophysics*, **629**:165-178. <https://doi.org/10.1016/j.tecto.2014.04.030>

- Macnae J. 1995. Applications of geophysics for the detection and exploration of kimberlites and lamproites. *Journal of Geochemical Exploration*, **53**(1-3):213-243. [https://doi.org/10.1016/0375-6742\(94\)00057-1](https://doi.org/10.1016/0375-6742(94)00057-1)
- Menegotto E., Medeiros E.R. 1976. Contribuição ao estudo das rochas ígneas ácidas da região da Serra Tupanci-RS. In: Congresso Brasileiro de Geologia. *Anais...*, **29**:427-432.
- Minty B.R.S. 1997. Fundamentals of airborne gamma-ray spectrometry. *AGSO Journal of Australian Geology and Geophysics*, **17**(2):39-50.
- Müller I.F., Nardi L.V.S., Lima E.F., Mexias A.S. 2012. Os diques latíticos portadores de ouro e sulfetos da associação shoshonítica de Lavras do Sul - RS: Petrogenese e geoquímica. *Pesquisas em Geociências*, **39**(2):173-191. <https://doi.org/10.22456/1807-9806.35911>
- Nabighian M.N. 1972. The analytic signal of two-dimensional magnetic bodies with polygonal cross-section: Its properties and use for automated anomaly interpretation. *Geophysics*, **37**(3):507-517. <https://doi.org/10.1190/1.1440276>
- Nabighian M.N., Ander M.E., Grauch V.J.S., Hansen R.O., LaFehr T.R., Li Y., Pearson W.C., Peirce J.W., Phillips J.D., Ruder M.E. 2005. Historical development of the gravity method in exploration. *Geophysics*, **70**(6):63ND-89ND. <https://doi.org/10.1190/1.2133785>
- Nagy D. 1966. The prism method for terrain corrections using digital computers. *Pure and Applied Geophysics*, **63**(1):31-39. <https://doi.org/10.1007/BF00875156>
- Nardi L.V.S. 1984. *Geochemistry and petrology of the lavras granite complex, RS, Brasil*. PhD Thesis, University of London, London, 268 p.
- Nardi L.V.S., Lima E.F. 1985. A associação shoshonítica de Lavras do Sul, RS. *Revista Brasileira de Geociências*, **15**(2):139-146. <https://doi.org/10.25249/0375-7536.1985139146>
- Nardi L.V.S., Lima E.F. 2000. O magmatismo shoshonítico e alcalino da Bacia do Camaquã - RS. In: Geologia do Rio Grande do Sul. *Anais...* Porto Alegre: CIGO/UFRGS, p. 119-131.
- Nardy A.J.R., Moreira C.A., Machado F.B., Luchetti A.C.F., Hansen M.A.F. 2014. Gamma-ray Spectrometry signature of Paraná Volcanic Rocks: preliminary results. *Geociências*, **33**(2):216-227.
- Nishad R., Sinha A., Kumaravel V., Patil S. 2013. Magnetic properties of dolerite dykes and lamprophyre sills from Jharia coal fields, Damodar valley basin, India. *Journal of Indian Geophysical Union*, **17**(4):341-348.
- Paim P.S.G., Chemale Jr. F., Lopes R. da C. 2000. A Bacia do Camaquã. In: Geologia do Rio Grande Do Sul. Porto Alegre: CIGO/UFRGS, p. 231-274.
- Paim P.S.G., Chemale Jr. F., Wildner W. 2014. Estágios evolutivos da Bacia do Camaquã (RS). *Ciência e Natura*, **36**(3):183-193. <https://doi.org/10.5902/2179460x13748>
- Parasnis D. 1973. Methods in geochemistry and geophysics. In: Parasnis D. (Ed.). *Mining geophysics*. Elsevier.
- Rao N.V.C. 2008. Petrophysical properties of indian kimberlites, lamproites and lamprophyres. In: Srivastava R.K., Sivaji C., Rao N.V.C. (Eds.). *Indian dykes: geochemistry, geophysics and geochronology*. New Delhi: Narosa Publishing House, p. 309-318.
- Ribeiro M. 1966. Geologia da quadrícula Caçapava do Sul, RS. *Boletim da Divisão de Fomento da Produção Mineral*, **127**, 232 p.
- Ribeiro M., Fantinel L.M.A. 1978. Associações petrotectônicas do escudo sul-riograndense: I tabulação e distribuição das associações petrotectônicas do Escudo do Rio Grande do Sul. *Iheringia, Série Geológica*, **5**(1):19-54.
- Rock N.M.S. 1991. Lamprophyres. Boston: Springer. <https://doi.org/10.1007/978-1-4615-3924-7>
- Rymer H., Brown G.C. 1986. Gravity fields and the interpretation of volcanic structures: Geological discrimination and temporal evolution. *Journal of Volcanology and Geothermal Research*, **27**(3-4):229-254. [https://doi.org/10.1016/0377-0273\(86\)90015-6](https://doi.org/10.1016/0377-0273(86)90015-6)
- Seedorff E., Dilles J.H., Proffett J.M.J., Einaudi M.T., Zurcher L., Stavast W.J.A., Johnson D.A., Barton M.D. 2005. Porphyry deposits: characteristics and origin of hypogene features. *Society of Economic Geologists*, **100**:251-298.
- Segev A., Rybakov M., Tuvia W., Beyth M. 1993. Lower Cretaceous magmatic body in the Timna Valley: magnetometric interpretation. *Israel Geological Survey Current Research*, **8**:21-23.
- Sharma P.V. 1997. *Environmental and engineering geophysics*. Cambridge: Cambridge University Press, 499 p.
- Shives R., Charbonneau B., Ford K. 2000. The detection of potassic alteration by gamma-ray spectrometry—Recognition of alteration related to mineralization. *Geophysics*, **65**(6):2001-2011. <https://doi.org/10.1190/1.1444884>
- Sommer C.A., Lima E.F., Pierosan R., Machado A. 2011. Reoignimbritos e ignimbritos de alto grau do vulcanismo Acampamento Velho, RS: origem e temperatura de formação. *Revista Brasileira de Geociências*, **41**(3):420-435. <https://doi.org/10.25249/0375-7536.2011413420435>
- Štemprok M., Seifert T. 2011. An overview of the association between lamprophyric intrusions and rare-metal mineralization. *Mineralogia*, **42**(2-3):121-162. <https://doi.org/10.2478/v10002-011-0011-x>
- Streckeisen A. 1979. Classification and nomenclature of volcanic rocks, lamprophyres, carbonatites, and melilitic rocks: Recommendations and suggestions of the IUGS Subcommission on the Systematics of Igneous Rocks. *Geology*, **7**(7):331-335. [https://doi.org/10.1130/0091-7613\(1979\)7%3C331:CANOVR%3E2.0.CO;2](https://doi.org/10.1130/0091-7613(1979)7%3C331:CANOVR%3E2.0.CO;2)
- Taylor W.R., Rock N.M.S., Groves D.I., Perring C.S., Golding S.D. 1994. Geochemistry of Archean shoshonitic lamprophyres from the Yilgarn Block, Western Australia: Au abundance and association with gold mineralization. *Applied Geochemistry*, **9**(2):197-222. [https://doi.org/10.1016/0883-2927\(94\)90007-8](https://doi.org/10.1016/0883-2927(94)90007-8)
- Tenzer R., Sirguyev P., Rattenbury M., Nicolson J. 2011. A digital rock density map of New Zealand. *Computers & Geosciences*, **37**(8):1181-1191. <https://doi.org/10.1016/j.cageo.2010.07.010>
- Wildner W., Lima E.F., Nardi L.V.S., Sommer C.A. 2002. Volcanic cycles and setting in the Neoproterozoic III to Ordovician Camaquã Basin succession in southern Brazil: Characteristics of post-collisional magmatism. *Journal of Volcanology and Geothermal Research*, **118**(1-2):261-283. [https://doi.org/10.1016/S0377-0273\(02\)00259-7](https://doi.org/10.1016/S0377-0273(02)00259-7)
- Wilford J.R. 2002. Airborne gamma-ray spectrometry. In: Papp E. (Ed.). *Geophysical and remote sensing methods regolith exploration*. CRCLEME Open File Report, **144**:46-52.
- Wilford J.R., Bierwirth P.N., Craig M.A. 1997. Application of airborne gamma-ray spectrometry in soil/regolith mapping and applied geomorphology. *AGSO Journal of Australian Geology and Geophysics*, **17**(2):201-216.
- Zuo L., Pei R., Shuai K., Yang F., Zhu R., Zhang L. 2011. Geochemistry of ore-bearing lamprophyre from the Cu-Ni deposit in Dhi Samir, Yemen. *Acta Geologica Sinica*, **85**(1):200-210. <https://doi.org/10.1111/j.1755-6724.2011.00390.x>
- Zuzana S., Vladislav R., Bedřich M. 2009. Effect of small potassium-rich dykes on regional gamma-spectrometry image of a potassium-poor volcanic complex: A case from the Doupské hory Volcanic Complex, NW Czech Republic. *Journal of Volcanology and Geothermal Research*, **187**(1-2):26-32. <https://doi.org/10.1016/j.jvolgeores.2009.07.018>